

Static finite element analysis of architectural glass curtain walls under in-plane loads and corresponding full-scale test

A.M. Memari[†], A. Shirazi[‡] and P.A. Kremer^{‡†}

*Department of Architectural Engineering, The Pennsylvania State University,
104 Engineering Unit A, University Park, PA 16802, U.S.A.*

(Received May 19, 2004, Accepted December 26, 2006)

Abstract. A pilot study has been conducted to guide the development of a finite element modeling formulation for the analysis of architectural glass curtain walls under in-plane lateral load simulating earthquake effects. This pilot study is one aspect of ongoing efforts to develop a general prediction model for glass cracking and glass fallout for architectural glass storefront and curtain wall systems during seismic loading. For this study, the ANSYS finite element analysis program was used to develop a model and obtain the stress distribution within an architectural glass panel after presumed seismic movements cause glass-to-frame contact. The analysis was limited to static loading of a dry-glazed glass curtain wall panel. A mock-up of the glass curtain wall considered in the analysis with strain gages mounted at select locations on the glass and the aluminum framing was subjected to static loading. A comparison is made between the finite element analysis predicted strain and the experimentally measured strain at each strain gage location.

Keywords: curtain walls; architectural glass; seismic evaluation; finite element analysis; static test.

1. Introduction

Although standardized analysis and design methods for architectural glass wall systems subjected to out-of-plane loads due to wind are relatively well-developed (e.g., ASTM 2003, TISE 1999), analogous methods have not been developed for the analysis and design of these wall systems subjected to seismic loads. During seismic interstory drifts, conventionally constructed curtain wall framing is prone to racking that causes architectural glass panels to translate and rotate as rigid bodies within the frame. Experimental studies have shown that when the corners of one diagonal of a glass panel make contact with the deformed frame along its shorter diagonal during racking, additional interstory drift leads to glass fracture and perhaps even glass fallout under the in-plane compressive contact forces that are generated between the glass corners and the wall framing system corners. Thus, in cases where consideration of seismic effects is part of the design, curtain wall manufacturers typically try to satisfy seismic requirements by providing “adequate” glass-to-

[†] Ph.D., P.E., Associate Professor, Corresponding author, E-mail: amm@engr.psu.edu

[‡] Former Graduate Student

^{‡†} Research Associate

frame clearances (Beason and Lingnell 2000). This is done by specifying clearances that exceed a geometry-based prediction for glass-to-frame contact (Dowrick 2003, Memari *et al.* 2006). However, these clearances (typically 6 mm (1/4 in.) to 13 mm (1/2 in.)) sometimes lead to curtain wall designs that are inadequate for even moderate earthquakes because the interstory drift caused by such earthquakes can lead to glass panel movements relative to the framing that exceed the clearances and subject the glass panel to compression along a diagonal. In addition, often inadequate consideration is given to subsequent load interactions between the glass and frame in those cases where drifts are sufficient to overcome the glass-to-frame clearances.

These concerns about clearance-based design sometimes prompt architectural glass wall system manufacturers to conduct full-scale mock-up tests using laboratory test methods such as those developed and published by the American Architectural Manufacturer's Association (AAMA) (2001a, 2001b) to aid in the design of architectural glass wall systems to withstand seismic loads. Because seismic codes in the U.S. have only recently devised provisions for safeguarding curtain walls with architectural glass during earthquakes (Behr and Warner 2003), an obvious critical need also exists for evaluating the expected resistance to glass breakage during earthquakes for existing curtain walls.

Quite often the development of code provisions and test standards addressing a perceived problem leads to increased attention toward the development of analytical procedures. A review of the literature has indicated that to date, relatively few published works have addressed analytically the seismic in-plane structural behavior of architectural glass. Most recently, Sucuoglu and Vallabhan (1997) extended the work of Bouwkamp and Meehan (1960) by considering analytical procedures for "calculating the in-plane deformation capacity and out-of-plane resistance of window glass panels subjected to seismic excitation." TISE (1999) mentions a finite element modeling effort by Pilkington glass in evaluation of local stresses around a bolt hole for their Planar system of bolted glass support. However, no published work related to the use of finite element analysis capabilities to consider glazing systems under seismic loads has been found.

One reason for the lack of prior work in this area is the complex analysis problem that is a result of the interaction of several physical components that make up the curtain wall system (e.g., rubber gaskets, glass pane, aluminum framing) and its attachment to the structural system. Another reason is that curtain walls are generally classified as "nonstructural elements," which implies a lack of justification for the efforts required for advanced structural analysis. Nonetheless, as established in other areas of structural engineering, finite element modeling and analysis can provide an effective means to analyze existing and new curtain wall systems subjected to seismic loading and has been the subject of ongoing activities at the Pennsylvania State University. In fact, it may be possible for finite element formulations to supplement or perhaps in many cases replace mock-up testing. With these possibilities in mind, a pilot study was recently conducted to evaluate the strains in a dry-glazed architectural glass curtain wall system mock-up both analytically and experimentally. It should be noted that what is reported in this paper is not the result of a comprehensive experimental and analytical study. Rather, it is a pilot study to show the feasibility of the approach in developing finite element models of curtain wall systems and experimental measurement of strains in mockups. A more detailed treatment of the subject is planned for the continuation of the study. As a result, only one full-scale experiment with strain measurement is reported here. Determining the repeatability of the strain measurements was out of the scope of this pilot study. More tests will be carried out as the research develops further in the future. A comparison of the analytical and experimental results to assess the appropriateness of finite element modeling for seismic damage prediction (based on drift capacity) in dry-glazed architectural glass curtain walls is discussed in this paper.

2. Mock-up test

2.1 Test plan

The architectural glass curtain wall system considered in this study is the dry-glazed, Kawneer 1600™ wall system detailed in Fig. 1. This wall system is commonly used in mid-rise building construction and has been included in several dynamic racking studies due to the generic nature of its design. Because previous studies have shown its behavior to be very repeatable (Memari *et al.* 2003, 2004), 6 mm (1/4 in.) thick annealed (AN) monolithic architectural glass was used to construct the single mock-up used in this pilot study. Glass dimensions were chosen to allow later comparisons with data from previous studies conducted on similarly glazed specimens. The Kawneer 1600™ wall system uses rubber gaskets between the glass and the aluminum curtain wall frame and rubber gasket lined pressure plates to secure the glass panel perimeter. Rubber setting blocks were located at the quarter points to support the bottom horizontal glass edge, and rubber side spacers were located at mid-height of each vertical glass edge. The setting and side “blocking” are designed to cushion the glass panel and attempt to maintain the glass-to-frame edge clearance as the glass and frame move relative to one another during in-service conditions.

The curtain wall mock-up was subjected to static racking as depicted schematically in Fig. 2. The facility shown in Fig. 2, which is typically used for dynamic racking crescendo tests, is described in greater detail by Behr and Belarbi (1996) and in AAMA 501.6-01 (AAMA 2001b). The mock-up was centered between the sliding steel tubes of the test facility, and the vertical mullions were anchored at all four corners to the facility’s sliding steel tubes. These steel tubes slide on roller assemblies in opposite directions by means of a fulcrum and pivot arm mechanism. The bottom sliding steel tube was displaced monotonically by a computer controlled electro-hydraulic servoactuator at a slow rate of 0.01 cm/sec. Loads applied to the curtain wall mockup by the hydraulic actuator were acquired continuously by the load cell depicted in Fig. 2. Moreover,

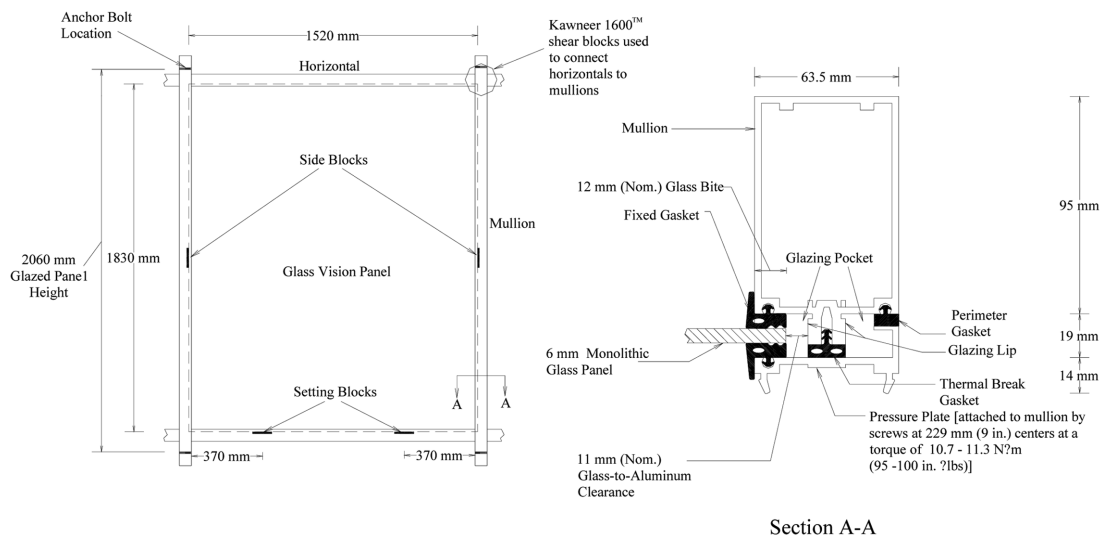


Fig. 1 General glazing details for curtain wall mock-up tested

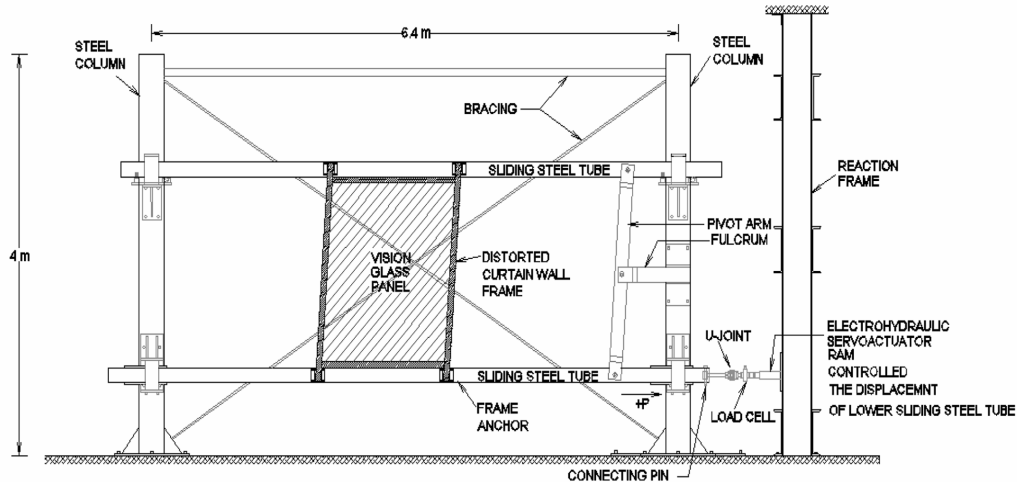


Fig. 2 Dynamic Racking Test Facility schematic

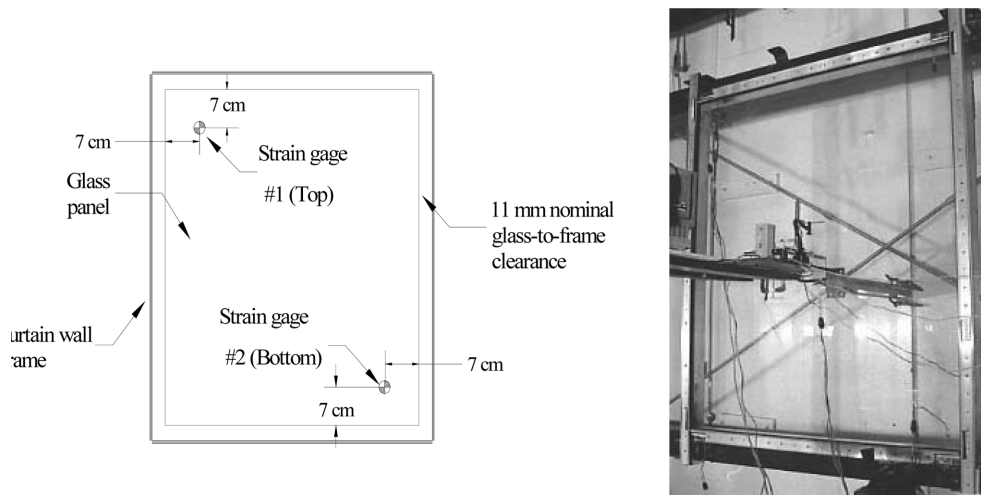


Fig. 3 Strain gage locations on architectural glass curtain wall mock-up

displacement of the hydraulic actuator was measured with the LVDT embedded in the actuator. The loading protocol was displacement controlled, and the actuator stroke was the same as the displacement of the top of the glazing frame. The measured load and displacement data were used to prepare the load-displacement relationship for the mock-up discussed later.

Because the objective of this experimental study was the measurement of strains at select locations in the glass panel, strain gages were employed at those locations shown in Fig. 3. Strain gage mounting locations were selected using results from the corresponding finite element analysis described later. Measurements Group CEA-06-125UR planar, rectangular strain gage rosettes were used to measure strains. Rosettes were bonded to the outside surface of the glass specimens and the glazing lip of the aluminum frame. Measurements Group 2120 strain gage conditioning amplifiers in a three-wire quarter bridge configuration were used to acquire strains from each gage. Principal

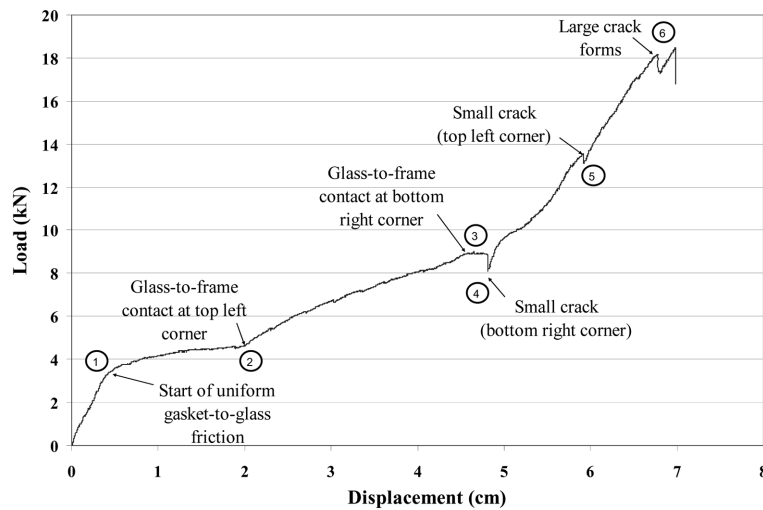


Fig. 4 Load-displacement relationship during static (0.01 cm/sec) racking test

strains and their directions for each rosette location were determined using standard strain gage rosette strain transformation relationships (Measurements Group 1990).

2.2 Load-displacement relationship

The acquired load-displacement relationship for the mock-up tested is shown in Fig. 4, which also identifies observed specimen behavior at various load/displacement levels. Initial resistance to distortion of the specimen shown schematically in Fig. 2 is comprised of aluminum curtain wall frame elastic stiffness and rubber gasket/blocking-to-glass surface friction, which is created by the pressure plate shown in Fig. 1. This pressure plate is attached to the aluminum frame by screws at 229 mm spacing and at a torque of 10.7-11.3 N·m, and as a result, it causes a large friction force between the glass panel edge and the rubber gasket.

Between Points 1 and 2, the load-displacement curve has a much smaller slope compared to the initial slope because this slope is essentially a measure of the frame stiffness after the frictional resistance between the glass panel edge and the rubber gasket was overcome (at Point 1 in Fig. 4). The corresponding load at the point where this friction force was overcome is about 4 kN (as shown in Fig. 4), and beyond this point, the friction did not contribute to the stiffness, i.e., the stiffness curve shown between Points 1 and 2 prior to first contact between glass and frame at a top corner (Point 2). In other words, after Point 1 and before Point 2, the stiffness of the framing components was the primary cause of the continued increase in load. Beyond Point 2, the glass at one corner (top left) was in contact with the frame and resulted in the stiffness increase (slope increase) between Points 2 and 3.

Continued distortion of the mock-up led to the second contact point at the bottom right corner shown as Point 3 in Fig. 4. At Point 4, localized glass crushing and flaking occurred in the bottom right corner and caused a momentary decrease in the measured load. Between Points 4 and 5, opposite corners of the glass plate (along the diagonal formed by the top left and lower right corners) were in contact with corresponding frame corners, and this interaction led to a further

increase in stiffness. Although the small crack that developed in the top left corner at Point 5 in conjunction with crushing and flaking in that corner caused another momentary decrease in the measured load, the stiffness from Point 4 up to Point 6 shown is relatively constant. It should be noted that the initial stiffness is slightly larger than the stiffness between points 4 and 6. As explained earlier, once the lateral load overcame the friction resistance, the stiffness observed was only due to the interaction of the glass panel and the glazing frame.

At Point 6, a major crack propagated through the glass thickness, which led to yet another decrease in the load level. Beyond Point 6, continued crushing, flaking and cracking in the corner regions continued with no significant increases in observed load. Because the objective of the experiment was to measure strains up to the point of cracking (which is an important indicator of a loss of serviceability in an architectural glass panel), the data beyond Point 6 were not relevant to this study and are not shown in Fig. 4.

3. Finite element modeling and analysis

To develop a realistic model of the interaction between glass panels and aluminum frame under dynamic racking displacement, both the rigid body movement of the glass and the deformation of the glass and frame after glass-to-frame contact must be considered. Furthermore, a refined model should consider the effect of gasket friction, frame deformation, as well as frame to structural connections. However, for the curtain wall mock-up considered in this study, certain simplifications were made consistent with the goal of the study, being only a pilot effort.

Accordingly, the load application for the experiment was limited to a static, monotonic lateral load. The rigid body movement of the glass panel within the aluminum frame before glass-to-frame contact at corners is generally resisted by the perimeter gasket friction. The resistance can be determined using experimental data during mock-up testing. Therefore, for simplicity of modeling, rigid body movement was not directly considered in the finite element model in this study. Instead,

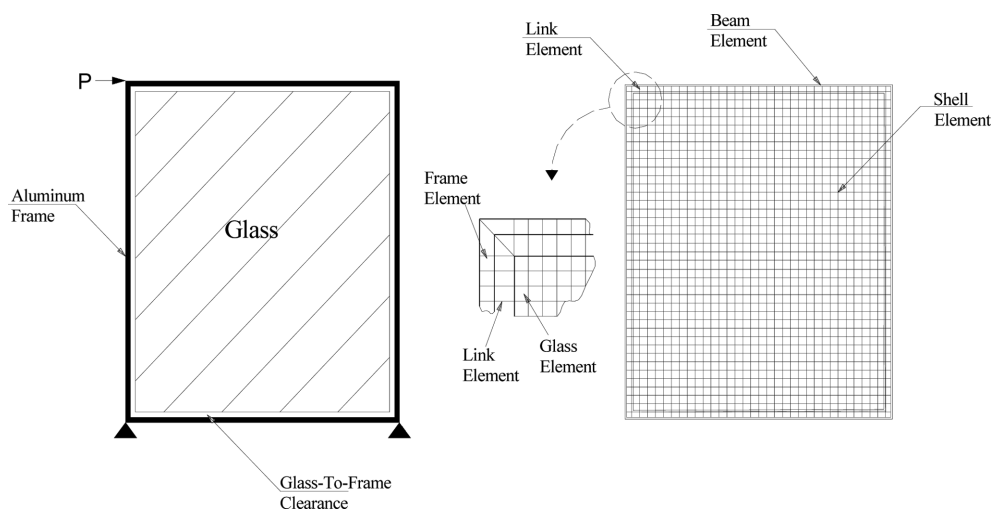


Fig. 5 Schematic diagram of applied load and mesh used for finite element model analysis

only glass and frame behavior after glass-to-frame contact at both corners of one diagonal have been included in the finite element modeling described below, i.e., the portion of Fig. 4 beyond Point 3. This restriction is consistent with the objective of the study, which was to correlate the strains measured at select locations of the glass panel during the mock-up test to corresponding strains resulting from the finite element modeling and analysis of the mock-up. Because the ultimate objective of the modeling efforts is to predict the onset of glass cracking in an architectural glass panel, strains that develop in the aluminum frame during glass-to-frame contacts were not considered.

Fig. 5 is a schematic representation of the finite element mesh and the presumed glass loading developed for the ANSYS (Swanson Analysis System 2000) finite element analysis of the curtain wall system mockup shown in Fig. 1. Several types of finite elements were used to model the curtain wall mockup including the glass panel, glazing frame, and glass to frame connection. Four-node shell elements (SHELL 63) with six degrees of freedom per node were used to model the glass panel. Aluminum frame members were modeled using two-node beam elements (BEAM 3) with two planar translation degrees of freedom and one planar rotational degree of freedom per node. Finally, two-node link elements (LINK 10) with three planar degrees of freedom per node were used to model the glass-to-frame interface. These compression-only link (truss) elements were used because there is either contact (compression) or separation between glass and frame. This link element utilizes a bilinear stiffness property, which can model a uniaxial compression-only (or tension-only) condition. The element stiffness property is effective only in compression or only in tension (as chosen), and if used as a compression element, it will simulate separation (gap between glass-and-frame) when the element undergoes tension. As depicted in Fig. 5, hinge supports were provided at corner nodes on the bottom frame member.

The experimentally determined stiffness of the glazing lip in Fig. 1 (Memari *et al.* 2000) was used for the link element stiffness. This stiffness accounts for the torsional stiffness due to the eccentric action of the glass panel on the glazing lip of the horizontal frame members. The flexural stiffness of the aluminum frame is based on its section properties, which for this preliminary analysis were computed by assuming the frame cross-section to be a rectangular (95 mm × 63 mm) tubular section with a wall thickness of 2.3 mm. The following constants were used in the analysis: for the glass panel, E (modulus of elasticity) = 72 GPa, ν (Poisson's ratio) = 0.25, ρ (mass density) = 2500 kg/m³; for the aluminum frame, E = 69 GPa, ν = 0.33, ρ = 2700 kg/m³; for the rubber blocking, E = 0.003 GPa.

4. Accounting for the effect of perimeter gaskets and blocking

4.1 Descriptions of corrections needed for comparison of finite element analysis and experimental results

As shown in Section A-A of Fig. 1, fixed rubber gaskets attached to the aluminum frame clamp the glass panel in place and help to restrict out-of-plane movement along the panel's edges. The gaskets distribute the confining pressure resulting from pressure plate screw tightening on both faces of the glass panel along its perimeter. When the glass panel is subjected to in-plane load, some resistance to translation and rotation of the glass panel within the aluminum frame "glazing pockets" results from the frictional force developed at the glass-to-gasket/blocking interface. This

frictional force combined with the unglazed (i.e., with no glass or gasket/blocking) or “bare” aluminum frame resistance forms the overall resistance to in-plane racking displacement of the mock-up shown schematically in Fig. 2 before glass-to-frame contact (as assumed in finite element modeling) is realized.

If the load read from the load cell during the experiment is used as input for the finite element analysis of the mock-up, the resulting strains computed by the finite element model will overestimate those strains measured experimentally during the mock-up test. For a correct comparison, it is necessary to determine that contribution to the measured load that can be attributed to bare frame resistance and the portion that can be attributed to gasket/blocking friction. Thus, the correct load to be applied to the finite element model is the net load obtained by subtracting the latter two loads (bare frame resistance and gasket/blocking friction) from the measured load.

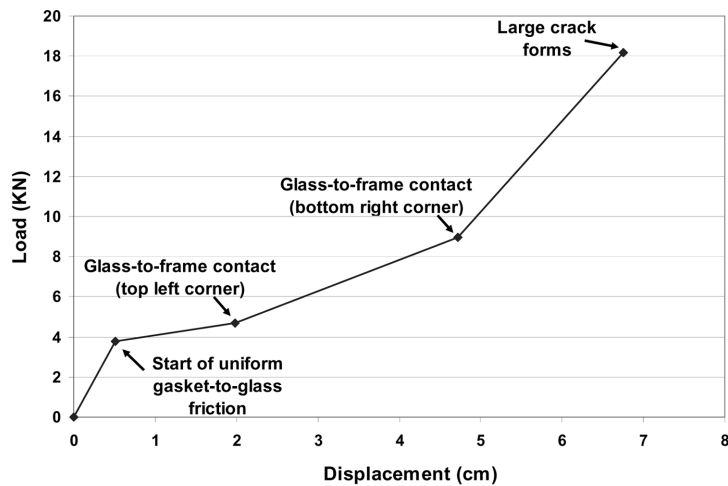


Fig. 6 Simplified load-displacement relationship during static (0.01 cm/sec) racking test

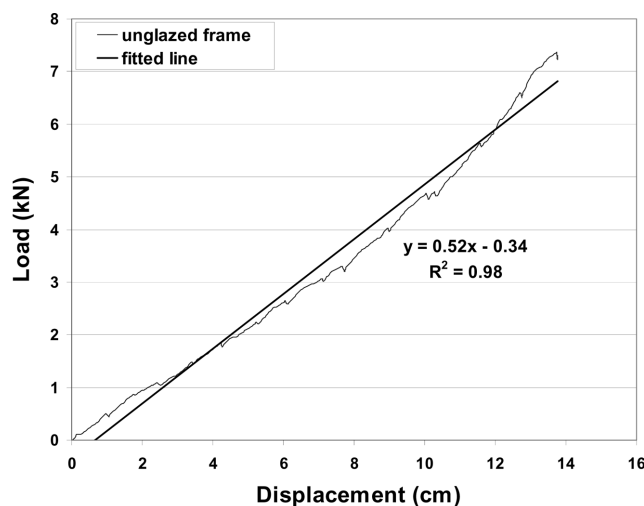


Fig. 7 Load-displacement relationship during static (0.01 cm/sec) racking of unglazed curtain wall frame

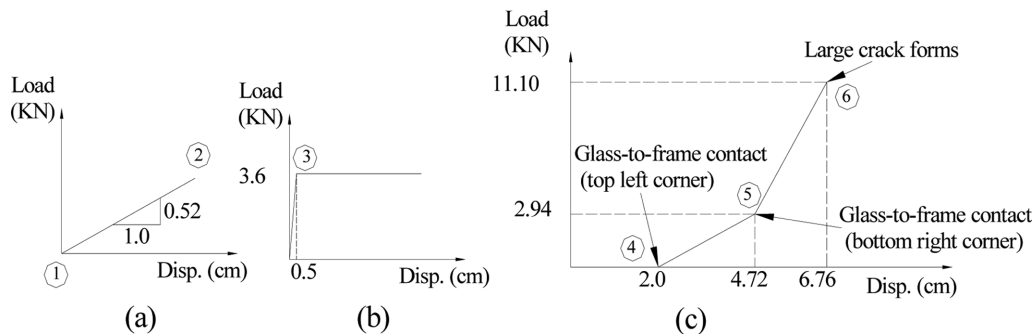


Fig. 8 Simplified load-displacement relations: (a) unglazed frame, (b) uniform gasket/blocking-to-glass friction, (c) after first glass-to-frame contact

Although the magnitude of corrections mentioned may be small in some cases, they are included in this discussion because the objective is to develop the procedure to account for them as needed. Furthermore, the strains computed by finite element analysis using this corrected load represent the strains that would result due to the glass-to-frame contact force. For comparison of experimentally measured and analytically calculated strains, it is also necessary to subtract from the measured strains that portion attributed to gasket/blocking friction.

To aid in correction of the applied load input to the model, it is convenient to approximate the load-displacement relationship from the mock-up test (Fig. 4) by a series of straight lines as shown in Fig. 6. Stiffness coefficients can then be easily defined using Fig. 6. A separate load-displacement relationship for a bare frame was also obtained experimentally using the previously described procedure for the mock-up test. This relationship is shown in Fig. 7 along with a linear fit and is used to account for that portion of the load attributed to bare frame resistance.

The end result of subtracting the contribution of the framing and the gasket/blocking from the load-displacement relationship for the mock-up test is shown graphically in Fig. 8. Fig. 8(a) is the linear fit for the bare frame from Fig. 7, and Fig. 8(b) is an idealized load-displacement relationship for the gasket/blocking. Fig. 8(b), assumes that gaskets resist the in-plane movement of the glass plate linearly before slip occurs (i.e., before Point 1 in Fig. 4) and that beyond this point, the resistance is essentially constant (in this case 3.6 KN). Fig. 8(c) is the end result of subtracting the bare frame and gasket/blocking contributions (Figs. 8(a) and 8(b)) from Fig. 6, and represents the mock-up load-displacement relationship after glass-to-frame contact is realized and up to the point of glass cracking. Fig. 8(c) shows that about 2.0 cm displacement is required before first contact occurs between the top left corner of the glass panel and the corresponding corner of the aluminum frame. Moreover, Fig. 8(c) shows that about 4.7 cm of displacement is required before glass-to-frame contact along both corners of the diagonal formed by the top left corner and the bottom right corner of the mock-up is realized. This agrees well with the predicted 4.8 cm displacement (Memari *et al.* 2006) for contact along a diagonal for the 11 mm nominal glass-to-frame clearance used for this mock-up.

4.2 Development of expressions for load and strain corrections

Based on the foregoing discussion, expressions need to be developed for load and strain

corrections. The expression for the load applied to the mock-up at any point during the mock-up test consists of three components, which represent the resistances experienced. These resistances can be thought of as parallel springs. The total resistance then consists of the following components:

$$P_{total}^T = P_{glass\ contact}^T + P_{frame}^T + P_{gasket/blocking}^T \quad (1)$$

The superscript T refers to loads associated with the mock-up test; thus, P_{total}^T is the total load applied to the frame by the hydraulic actuator of the racking facility (Fig. 2) during the test. P_{total}^T is comprised of $P_{glass\ contact}^T$, that portion of the total load transferred to the glass panel during glass-to-frame contact; P_{frame}^T , that portion of the total load attributed to pure frame resistance (deformation prior to glass-to-frame contact); and $P_{gasket/blocking}^T$, that portion of the total load attributed to gasket/blocking-to-glass frictional forces.

An expression similar to Eq. (1) can be written for the finite element analysis of the mock-up; however, because gasket/blocking friction is not considered in the analysis, a gasket/blocking friction term is not included (the superscript A refers to the analysis results):

$$P_{total}^A = P_{glass\ contact}^A + P_{frame}^A \quad (2)$$

Using the linear approximations of stiffness coefficients from the load-displacement relationship for the mock-up test, P_{total}^A can be expressed in terms of total frame lateral displacement (D_{total}^A) and the stiffness coefficients for glass contact ($K_{glass\ contact}^A$) and bare frame (K_{frame}^A), as follows:

$$P_{total}^A = K_{total}^A D_{total}^A \quad (3)$$

$$K_{total}^A = K_{glass\ contact}^A + K_{frame}^A \quad (4)$$

Eq. (4) assumes that the frictional resistance provided by gasket/blocking is constant once the glass panel starts to slip with respect to the gaskets, i.e., the stiffness provided by gasket/blocking is zero once slip starts as idealized in Fig. 8(b). Eq. (4) describes the total stiffness after glass-to-frame contact and makes no distinction between the stiffness when only one corner of the glass panel contacts the frame or when both corners of a glass panel diagonal contact the frame. However, Fig. 8(c) shows that the latter case results in a higher stiffness. Glass cracking for most glass types and framing configurations typically occurs after glass-to-frame contact takes place at both corners along a diagonal, although in some cases such as AN monolithic glass, cracking can initiate after glass-to-frame contact in only one corner. Given that the main objective of this analysis effort was the determination of the magnitude of the compressive strain expected to initiate cracking in the glass panel and the fact that the finite element model represents the condition that both opposite corners of a glass panel are in contact with the frame pocket corners, the stiffness corresponding to the case of glass contact at both corners was used for computation of the contact glass load. Alternatively one could either use the stiffness corresponding to the first corner contact (line connecting points 4 and 5 in Fig. 8(c)) or the average of the two stiffness coefficients. However, as is discussed next, the load $P_{glass\ contact}^T$ is used to determine P_{total}^A and in that sense, it is the choice of which load not stiffness that is important, i.e., the load corresponding to the first contact (point 4) or second contact (point 5) in Fig. 8(c).

With the assumption that glass and frame lateral displacements resulting from the analysis are the same, i.e., $D_{total}^A = D_{glass\ contact}^A = D_{frame}^A$, individual force-displacement relations can be written as follows:

$$D_{total}^A = \frac{P_{total}^A}{K_{glass\ contact}^A + K_{frame}^A} = \frac{P_{glass\ contact}^A}{K_{glass\ contact}^A} = \frac{P_{frame}^A}{K_{frame}^A} \quad (5)$$

Thus, Eq. (3) becomes:

$$P_{total}^A = K_{total}^A D_{total}^A = K_{total}^A \times \frac{P_{glass\ contact}^A}{K_{glass\ contact}^A} \quad (6)$$

Writing $K_{glass\ contact}^A$ in terms of K_{total}^A and K_{frame}^A , we thus obtain Eq. (7):

$$P_{total}^A = \frac{K_{total}^A}{K_{total}^A - K_{frame}^A} P_{glass\ contact}^A \quad (7)$$

As previously discussed, it is desirable for $P_{glass\ contact}^A$ to be the same as $P_{glass\ contact}^T$, which is obtained from the mock-up test. Hence, the applied load for the finite element modeling is adjusted by substituting $P_{glass\ contact}^T$ for $P_{glass\ contact}^A$ in Eq. (7), and K_{total}^A and K_{frame}^A can be obtained based on the finite element modeling. With this substitution, the $(K_{total}^A)/(K_{total}^A - K_{frame}^A)$ term can be viewed as a correction factor for $P_{glass\ contact}^T$. The correction factor is necessary to obtain the correct input for the finite element analysis in order to have the same state of stress in the test and in the finite element analysis.

The correction factor is then computed for the mock-up using the following finite element results: $K_{total}^A = 294$ KN/cm, $K_{frame}^A = 4.3$ KN/cm. This gives the correction factor of $(K_{total}^A)/(K_{total}^A - K_{frame}^A) = 1.015$. Moreover, from Fig. 8(c), $P_{glass\ contact}^T = 11.1$ KN at the crack initiation point. Thus, the corrected input load corresponding to glass cracking for the finite element analysis is $P_{total}^A = 1.015(11.1) = 11.3$ KN.

Because gasket/blocking friction was not considered in the finite element model, for a valid comparison of experimentally measured and analytically calculated strains, it was also necessary to subtract from the measured strains that portion attributed to gasket/blocking friction. The gasket/blocking frictional force can be assumed constant once relative movement between the glass panel and the gasket/blocking (slip) occurs, and it is also appropriate to assume that strains in the glass caused by these frictional forces also remain constant in magnitude. Strains in the glass panel can be assumed to be comprised of strains attributed to compression of the panel after the corners along one of the panel's diagonals contact the frame and strains attributed to the gasket/blocking frictional force. The strain measured in the branch "i" strain gage of the rosette used can thus be expressed as follows:

$$\varepsilon_{i,total}^T = \varepsilon_{i,glass\ contact}^T + \varepsilon_{i,gasket/blocking}^T \quad (8)$$

where $\varepsilon_{i,total}^T$ is the strain measured when there is glass-to-frame contact along a diagonal and before crack initiation and $\varepsilon_{i,gasket/blocking}^T$ is the strain measured before glass-to-frame contact. For rectangular rosettes used in the mock-up test, the principal strain for each rosette can be obtained as follows:

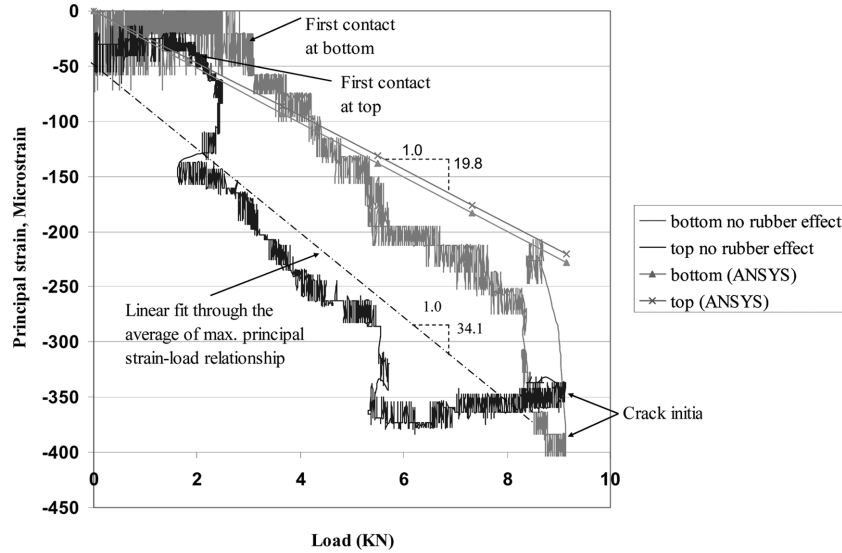


Fig. 9 Maximum principal strain versus contact load

$$\varepsilon_{p,q} = \frac{\varepsilon_1 + \varepsilon_3}{2} \pm \sqrt{((\varepsilon_1 - \varepsilon_2)^2 + (\varepsilon_2 - \varepsilon_3)^2)/2} \quad (9)$$

where $\varepsilon_{p,q}$ are the principal strains corresponding to glass contact, and $\varepsilon_1, \varepsilon_2, \varepsilon_3$ are strains in the three branches of the rosette. It should be noted that it is assumed here that the positive sign in Eq. (9) is taken for the larger principal strain. In other words, we assume here that ε_p is the maximum and ε_q is the minimum strain.

5. Comparison of mock-up test and analysis results

Fig. 9 is a plot of ε_p , the maximum in-plane principal strain, versus contact load for the top and bottom rosette locations with the effect of gasket/blocking friction removed per Eq. (8). The figure shows that the measured strains for the top rosette are larger (in magnitude) than those for the bottom rosette. This is related to the fact that glass-to-frame contact occurred at the top left corner of the glass panel first. For both the top and bottom rosettes, a sudden increase in slope (stiffness) of the load-strain relation occurs after glass-to-frame contact is made at the glass panel corner near the rosette. Plots of ε_p computed by finite element analysis for both the top and bottom rosette locations are also presented in Fig. 9.

As mentioned before, the first contact occurred at the top corner of the glass panel (Point 4 in Fig. 8(c)) in the test reported here, which results in load transfer to the glass panel and corresponding increases in measured strain magnitude. With increasing displacement (load), the bottom corner overcame the clearance between the glass panel edges and the frame pocket. After the second corner contact (Point 5 in Fig. 8(c)) the glass panel in the mock-up was subjected to the diagonal loading simulated by the finite element model. For this reason, maximum principal strains resulting from the analysis corresponded to the condition beyond Point 5 in Fig. 8(c), and are to

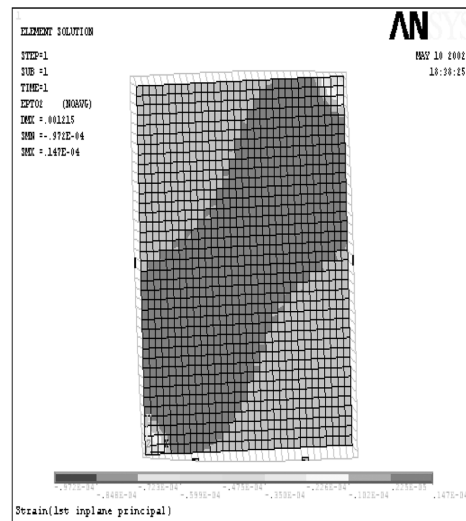
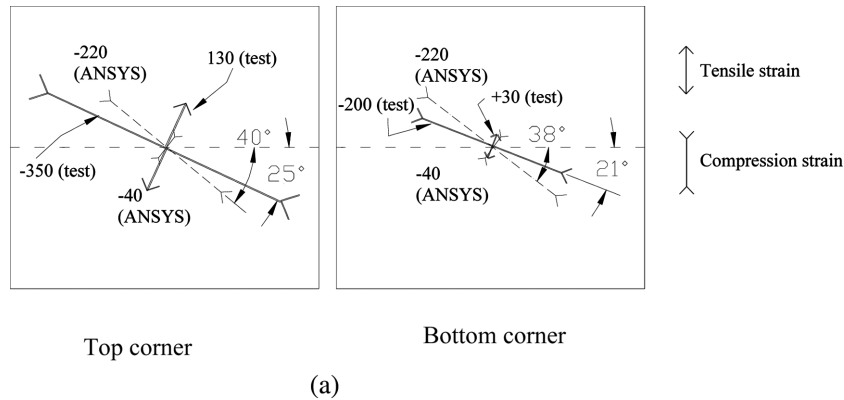


Fig. 10 (a) Comparison of the test and the ANSYS finite element analysis results (Note: Lines for reported strains are scaled relative to each other. Angles are measured from the principal strain direction to the horizon line), (b) Distribution of principal strain at cracking load from finite element analysis (Note: Color contours shows the distribution of the first principal strain)

some degree in agreement with the strains measured at the bottom rosette location. Beyond about 5 kN, strains measured at the bottom and strain at the top rosette are very different from FEM results, which is the result of continual glass damage (crushing and cracking) occurring at both corners beyond this point. It should be noted that the strains measured are of course the realistic strains for the mockup tested. The strains resulting from the finite element analysis are different from the test results because of the simplifications in the finite element modeling, including the assumption that the contact points are exactly the corner points. In reality, the contact points are not the exact corner points.

Strains measured up to 2 kN are almost constant. Strains up to this point are generated by friction between the gasket/blocking and the glass panel. The connections of aluminum frame members in the mock-up had some rigidity for frame action, but not to a degree to prevent member rotations at

Table 1 Comparison of analytical and experimental minimum and maximum principal strains and their orientations at the initiation of glass cracking

	Test top	FEA top	Test bottom	FEA bottom
ε_p (maximum principal strain)	+125.8	-39	+30.2	-37.5
ε_q (minimum principal strain)	-345.7	-217	-202.7	-224
ϕ (angle between maximum principal strain and rosette reference grid)	25.4	40.1	21.1	38.5

the joints. In the finite element model, however, the joints have been modeled as rigid connections, with the result of making the frame stiffer than the actual frame. The smaller stiffness and maximum principal strains generated in the finite element model of the glass panel as compared with the measured values at the top (Fig. 9) can be attributed to this effect. Such a difference is also generally expected because finite element models are usually stiffer than their equivalent physical systems as a result of using fewer degrees of freedom in the finite element model.

As described previously, the applied load to the finite element model was 11.3 kN, which includes the correction applied to 11.1 kN (Fig. 8c), the observed lateral load in the mock-up test corresponding to glass cracking. Fig. 10(a) and Table 1 present the experimental and analytical maximum and minimum in-plane principal strains (ε_p and ε_q) corresponding to crack initiation in the glass panel. As mentioned before, it should be noted that ε_p and ε_q are defined here as the maximum and minimum principal strains, respectively, are based on the Eq. (9). The acute angle from the principal axis to the reference grid for each rosette is presented in Fig. 10(a) and Table 1. The distributions of principal strains in the finite element model corresponding to crack initiation are shown in Fig. 10(b). The magnitude and direction of the experimental and analytical maximum principal strains are comparable and particularly close for the bottom rosette location. The primary reason for the difference in experimental and analytical principal strain values is that the finite element model simulates both corners in contact with the frame simultaneously, which results in analytically computed strains for the top and the bottom rosette locations that are approximately the same at any load level. However, the load-displacement relation in Fig. 4 shows that the loading of the glass panel is more complex because of the effects of gasket/blocking friction and that the load levels for the top and bottom corner contact points are not the same. Actual frame connections are semi-rigid, yet those connections have been modeled as rigid connections in the FEM. Because the stiffness beyond the bottom corner contact point is used for the finite element model, the finite element model strain approximations are closer to the principal strains corresponding to the bottom corner rosette location than to the strains corresponding to the top corner rosette location. Contacts between the corners of the glass panel and frame pocket sometimes cause a local plastic deformation in the mullion lip. This deformation provides a wider contact area. Therefore, the contact at the corners does not occur at a distinct point as assumed in the finite element model formulation. The other difference between the finite element model and the mock-up test is in the frame-to-building connections. The connection between the frame and racking facility is also semi-rigid. However, the frame-to-building connection model is assumed rigid in the finite element model. These additional differences between FEM and reality also contribute to some of the differences between the test and analysis results.

6. Estimation of edge cracking stress

Given that cracking initiates at glass panel edges where measurement of strains at cracking is difficult, it is desirable to develop a relationship between strains at the edges and strains at interior points where measurement has been made using a relationship obtained from the finite element modeling analysis results. A linear fit through the average of the maximum principal strain-load relationships presented for the top and bottom rosette locations is shown in Fig. 9. In addition, the results of finite element analysis show that the maximum principal strain at the glass edge at the points of glass-to-frame contact in each corner is “2.256” times greater than the maximum principal strain at the rosette strain gage locations in the finite element model. For simplicity, it was assumed that the same proportion holds between the maximum principal strains at the rosette locations in the mock-up and the edge of the glass where cracking initiates. Accordingly, the maximum principal strain at the edge in the mock-up, $\epsilon_{p,edge}$, can be approximated using Eq. (10).

$$\epsilon_{P,edge}(\text{microstrain}) = -77P_{contact}(KN) \tag{10}$$

The multiplier “77” in Eq. (10) was derived by multiplying the rosette location-to-edge strain factor (2.256 in this case) by the slope of the average strain-load relationship in Fig. 9, i.e., $2.256 \times 34.1 = 77$, and $P_{contact}$ in Eq. (10) is the glass-to-frame contact load at the glass edge location. It should be emphasized that because of the complex problem of glass to frame contact, the linearized relationship assumed in deriving the above values should be refined to develop a more accurate transformation between the edge strain and the rosette location point.

A similar relationship, however, cannot be developed for the minimum principal strain at the glass edge, $\epsilon_{q,edge}$ because the gasket friction, which is the primary source of the minimum principal strain, is not considered in the finite element model. To estimate glass panel edge principal stresses

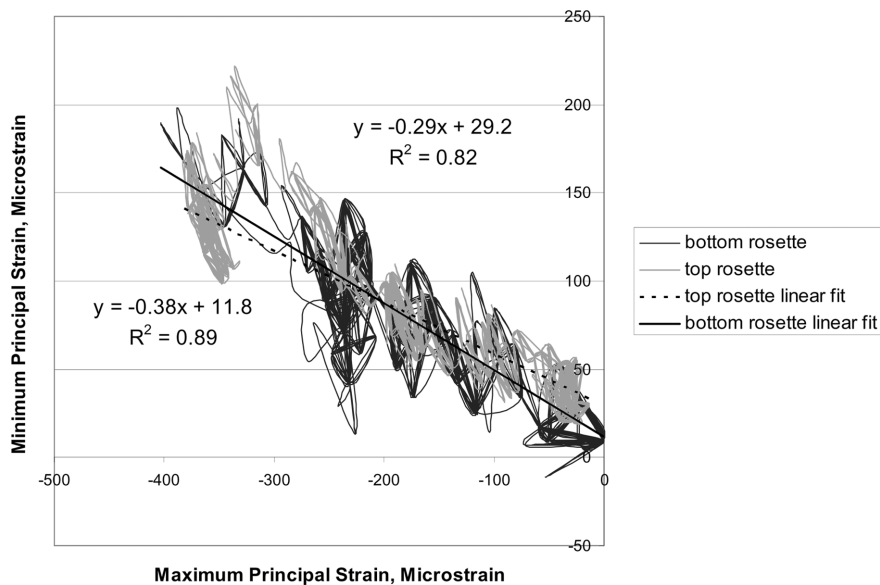


Fig. 11 Relation between principal strains at rosette strain gage locations

at the time of cracking, stress-strain relationships are needed. Eq. (11) shows the relationship between the strains and stresses where “ E ” is the glass modulus of elasticity and “ ν ” is the Poisson’s ratio of the glass.

$$\begin{bmatrix} \sigma_1 \\ \sigma_2 \end{bmatrix} = \frac{E}{1 - \nu^2} \begin{bmatrix} 1 & \nu \\ \nu & 1 \end{bmatrix} \begin{bmatrix} \varepsilon_{q,edge} \\ \varepsilon_{p,edge} \end{bmatrix} \quad (11)$$

As Eq. (11) shows, both principal edge strains are needed in order to calculate the glass panel edge stress. This problem can be resolved by using the average linear fit relating the maximum and minimum principal stresses for the top and bottom rosette locations measured during the mock-up test as shown in Fig. 11. As shown in Fig. 11, the linear fit provides a good estimate through the principal strain data. Eq. (12) shows the linear relationship between principal strains computed from Fig. 11.

$$\varepsilon_q = -0.34\varepsilon_p + 20.5 \quad (12)$$

If it is also assumed that Eq. (12) holds when relating minimum and maximum principal strains at the glass edge during contact, then substitution of $\varepsilon_{p,edge}$ from Eq. (10) into Eq. (12) gives an estimate for $\varepsilon_{q,edge}$ that can be used in Eq. (11). Most significantly, Eq. (11) can provide an estimate for principal stresses at crack initiation when $\varepsilon_{p,edge}$ and $\varepsilon_{q,edge}$ correspond to the principal strains at crack initiation.

Maximum principal strain generated at the corner of a glass panel due to a contact load can be calculated by the use of Eq. (10). Eq. (12) can be used to calculate the other (minimum) principal strain. Corresponding stresses generated in the corner of the glass can be calculated by using Eq. (11). The relations developed in this section then make it possible to estimate glass panel edge stresses at cracking state. This can be useful in developing a predictive model for architectural glass failure.

7. Conclusions

This study has addressed for the first time the complex problem of the interaction of a rigid glass panel and flexible aluminum framing through finite element modeling. The use of finite element modeling has been shown as a viable method to provide the tools to predict the state of stress in a curtain wall glass panel mock-up once glass-to-frame contact is initiated during racking. The study has defined the important parameters that can affect the response of a curtain wall mock-up and has illustrated how to adjust the finite element analysis input and the experimental output from instrumented mock-up tests to develop reasonable comparisons between the two. Of particular importance when adjusting the model are the role of gasket friction and the unglazed aluminum frame. The study has also shown how principal strains measured on the face of a glass panel during a mock-up test can be approximately related to those at the corner contact points along its edges. In addition, the results of this study suggest an approximate linear relationship between maximum and minimum principal strains.

Although this pilot study was limited in scope, it is expected that further research will lead to improved correlations between stresses and strains resulting from detailed finite element modeling

and analysis and full-scale mock-up tests. In particular, appropriate modeling of aluminum frame-to-structural frame connections, aluminum frame member-to-member connections and gasket-to-glass and gasket-to-frame contact is necessary for improved accuracy of the overall finite element modeling. Of course, the results presented in this paper were based on simplifying assumptions in the finite modeling because of the complex nature of the components making up the curtain wall and its attachment to the structural system. The results in no way can be generalized for curtain wall behavior; rather, this paper has presented an approach toward the development of prediction models. The ultimate objective is the development of a reliable methodology for predicting the lateral load in a glass panel at cracking. The results of finite element modeling can be used in development of a predictive model for seismic induced failure of architectural glass.

Acknowledgements

Partial funding for this study was provided by the National Science Foundation under Grant No. CMS-9983896. Support of NSF is gratefully acknowledged. Any opinions expressed here are those of the authors and do not necessarily represent those of National Science Foundation.

References

- American Architectural Manufacturers Association (AAMA). (2001a), Recommended Static Test Method for Evaluating Curtain Wall and Storefront Systems Subjected to Seismic and Wind Induced Interstory Drifts, AAMA 501.4-01.
- American Architectural Manufacturers Association (AAMA). (2001b), Recommended Dynamic Test Method for Determining the Seismic Drift Causing Glass Fallout from a Wall System, AAMA 501.6-01.
- American Society of Testing and Materials (ASTM). (2003), Standard Practice for Determining Load Resistance of Glass in Buildings, ASTM E 1300-03, West Conshohocken, PA.
- Beason, W.L. and Lingnell, W.A. (2000), "Chapter 8, emerging uses for window glass", *Emerging Materials for Civil Infrastructure State of the Art*, eds. R.A. Lopez-Anido and T.R. Naik, American Society for Civil Engineers, Reston, 190-216.
- Behr, R.A. and Belarbi, A. (1996), "Seismic test methods for architectural glazing systems", *Earthquake Spectra*, **12**(1), 129-143.
- Behr, R.A. and Warner, S. (2003), "Earthquake-resistant architectural glass new design provisions and test methods", *The Construction Specifier*, May 2003, 29-33.
- Bouwkamp, J.G. and Meehan, J.F. (1960), "Drift limitations imposed by glass", *Proc. of Second World Conf. on Earthquake Engineering*, Tokyo, Japan, 1763-1778.
- Dowrick, D.J. (2003), *Earthquake Risk Reduction*, West Sussex, John Wiley and Sons.
- Measurements Group. (1990), "Strain gage rosettes-selection, application and data reduction", *TN-515*, 1-10.
- Memari, A.M., Behr, R.A. and Kremer, P.A. (2000), "The role of small-scale tests of glass plates in seismic design of architectural glazing systems", *CD-ROM Proc., 12th World Conf. on Earthquake Engineering*, Auckland, New Zealand, 1-10.
- Memari, A.M., Behr, R.A. and Kremer, P.A. (2003), "Seismic behavior of curtain walls containing insulating glass units", *J. Arch. Eng.*, ASCE, **9**(2), 70-85.
- Memari, A.M., Kremer, P.A. and Behr, R.A. (2004), "Dynamic racking crescendo tests on architectural glass fitted with anchored "PET" film", *J. Arch. Eng.*, ASCE, **10**(1), 5-14.
- Memari, A.M., Kremer, P.A. and Behr, R.A. (2006), "Architectural glass panels with rounded corners to mitigate seismic damage", *Earthquake Spectra*, **22**(1), 129-150.

- Sucuoglu, H. and Vallabhan, C.V.G. (1997), "Behavior of window glass panels during earthquakes", *Eng. Struct.*, **19**(8), 685-694.
- Swanson Analysis Systems. (2000), ANSYS 5.0 User Manual – Procedures Vol. I.
- The Institute of Structural Engineers (TISE). (1999), *Structural Use of Glass in Buildings*, The Institute of Structural Engineers, London.